



Measurement of the Neutron Radius of ^{208}Pb through Parity Violation in Electron Scattering

S. Abrahamyan,³⁸ Z. Ahmed,²⁹ H. Albataineh,¹⁷ K. Aniol,² D. S. Armstrong,⁵ W. Armstrong,³¹ T. Averett,⁵ B. Babineau,¹⁹ A. Barbieri,³⁶ V. Bellini,¹¹ R. Beminiwattha,²³ J. Benesch,³² F. Benmokhtar,⁶ T. Bielarski,³⁴ W. Boeglin,⁷ A. Camsonne,³² M. Canan,²⁴ P. Carter,⁶ G. D. Cates,³⁶ C. Chen,⁸ J.-P. Chen,³² O. Hen,³⁰ F. Cusanno,^{13,†} M. M. Dalton,³⁶ R. De Leo,¹⁰ K. de Jager,^{32,36} W. Deconinck,^{21,5} P. Decowski,²⁸ X. Deng,³⁶ A. Deur,³² D. Dutta,²² A. Etile,¹⁷ D. Flay,³¹ G. B. Franklin,³ M. Friend,³ S. Frullani,¹³ E. Fuchey,^{4,31} F. Garibaldi,¹³ E. Gasser,¹⁷ R. Gilman,²⁶ A. Giusa,¹¹ A. Glamazdin,¹⁶ J. Gomez,³² J. Grames,³² C. Gu,³⁶ O. Hansen,³² J. Hansknecht,³² D. W. Higinbotham,³² R. S. Holmes,²⁹ T. Holmstrom,¹⁹ C. J. Horowitz,¹⁴ J. Hoskins,⁵ J. Huang,²¹ C. E. Hyde,^{24,4} F. Itard,¹⁷ C.-M. Jen,²⁹ E. Jensen,⁵ G. Jin,³⁶ S. Johnston,³³ A. Kelleher,²¹ K. Kliakhandler,³⁰ P. M. King,²³ S. Kowalski,²¹ K. S. Kumar,³³ J. Leacock,³⁷ J. Leckey IV,⁵ J. H. Lee,^{5,23} J. J. LeRose,³² R. Lindgren,³⁶ N. Liyanage,³⁶ N. Lubinsky,²⁵ J. Mammei,³³ F. Mammoliti,¹³ D. J. Margaziotis,² P. Markowitz,⁷ A. McCreary,³² D. McNulty,³³ L. Mercado,³³ Z.-E. Mezziani,³¹ R. W. Michaels,³² M. Mihovilovic,¹⁵ N. Muangma,²¹ C. Muñoz-Camacho,⁴ S. Nanda,³² V. Nelyubin,³⁶ N. Nuruzzaman,²² Y. Oh,²⁷ A. Palmer,¹⁹ D. Parno,³ K. D. Paschke,³⁶ S. K. Phillips,³⁴ B. Poelker,³² R. Pomatsalyuk,¹⁶ M. Posik,³¹ A. J. R. Puckett,²⁰ B. Quinn,³ A. Rakhman,²⁹ P. E. Reimer,¹ S. Riordan,³⁶ P. Rogan,³³ G. Ron,¹⁸ G. Russo,¹¹ K. Saenboonruang,³⁶ A. Saha,^{32,*} B. Sawatzky,³² A. Shahinyan,^{38,32} R. Silwal,³⁶ S. Sirca,¹⁵ K. Slifer,³⁴ P. Solvignon,³² P. A. Souder,^{29,‡} M. L. Spurduto,¹¹ R. Subedi,³⁶ R. Suleiman,³² V. Sulkosky,²¹ C. M. Suter,¹¹ W. A. Tobias,³⁶ W. Troth,¹⁹ G. M. Urciuoli,¹² B. Waidyawansa,²³ D. Wang,³⁶ J. Wexler,³³ R. Wilson,⁹ B. Wojtsekhowski,³² X. Yan,³⁵ H. Yao,³¹ Y. Ye,³⁵ Z. Ye,^{8,36} V. Yim,³³ L. Zana,²⁹ X. Zhan,¹ J. Zhang,³² Y. Zhang,²⁶ X. Zheng,³⁶ and P. Zhu³⁵

(PREX Collaboration)

¹Argonne National Laboratory, Argonne, Illinois 60439, USA

²California State University, Los Angeles, Los Angeles, California 90032, USA

³Carnegie Mellon University, Pittsburgh, Pennsylvania 15213, USA

⁴Clermont Université, Université Blaise Pascal, CNRS/IN2P3, Laboratoire de Physique Corpusculaire, FR-63000 Clermont-Ferrand, France

⁵College of William and Mary, Williamsburg, Virginia 23187, USA

⁶Christopher Newport University, Newport News, Virginia 23606, USA

⁷Florida International University, Miami, Florida 33199, USA

⁸Hampton University, Hampton, Virginia 23668, USA

⁹Harvard University, Cambridge, Massachusetts 02138, USA

¹⁰INFN, Sezione di Bari and University of Bari, I-70126 Bari, Italy

¹¹INFN, Dipt. di Fisica dell'Univ. di Catania, I-95123 Catania, Italy

¹²INFN, Sezione di Roma, I-00161 Rome, Italy

¹³INFN, Sezione di Roma, gruppo Sanità, I-00161 Rome, Italy

¹⁴Indiana University, Bloomington, Indiana 47405, USA

¹⁵Institut Jožef Stefan, 3000 SI-1001 Ljubljana, Slovenia

¹⁶Kharkov Institute of Physics and Technology, Kharkov 61108, Ukraine

¹⁷Laboratoire de Physique Corpusculaire, Clermont-Ferrand Campus des Cèzeaux, 63171 Aubière Cedex, France

¹⁸Lawrence Berkeley National Laboratory, Berkeley, California 94720, USA

¹⁹Longwood University, Farmville, Virginia 23909, USA

²⁰Los Alamos National Laboratory, Los Alamos, New Mexico 87545, USA

²¹Massachusetts Institute of Technology, Cambridge, Massachusetts 02139, USA

²²Mississippi State University, Mississippi State, Mississippi 39762, USA

²³Ohio University, Athens, Ohio 45701, USA

²⁴Old Dominion University, Norfolk, Virginia 23529, USA

²⁵Rensselaer Polytechnic Institute, Troy, New York 12180, USA

²⁶Rutgers University, The State University of New Jersey, New Brunswick, New Jersey 08901, USA

²⁷Seoul National University, Seoul 151-742, South Korea

²⁸Smith College, Northampton, Massachusetts 01063, USA

²⁹Syracuse University, Syracuse, New York 13244, USA

³⁰Tel Aviv University, P.O. Box 39040, Tel Aviv 69978, Israel

³¹Temple University, Philadelphia, Pennsylvania 19122, USA

³²Thomas Jefferson National Accelerator Facility, Newport News, Virginia 23606, USA

³³University of Massachusetts Amherst, Amherst, Massachusetts 01003, USA

³⁴*University of New Hampshire, Durham, New Hampshire 03824, USA*³⁵*University of Science and Technology of China, Hefei, Anhui 230026, People's Republic of China*³⁶*University of Virginia, Charlottesville, Virginia 22903, USA*³⁷*Virginia Polytechnic Institute and State University, Blacksburg, Virginia 24061, USA*³⁸*Yerevan Physics Institute, Yerevan, Armenia*

(Received 12 January 2012; published 15 March 2012)

We report the first measurement of the parity-violating asymmetry A_{PV} in the elastic scattering of polarized electrons from ^{208}Pb . A_{PV} is sensitive to the radius of the neutron distribution (R_n). The result $A_{PV} = 0.656 \pm 0.060(\text{stat}) \pm 0.014(\text{syst})$ ppm corresponds to a difference between the radii of the neutron and proton distributions $R_n - R_p = 0.33^{+0.16}_{-0.18}$ fm and provides the first electroweak observation of the neutron skin which is expected in a heavy, neutron-rich nucleus.

DOI: 10.1103/PhysRevLett.108.112502

PACS numbers: 21.10.Gv, 21.65.Ef, 25.30.Bf, 27.80.+w

Nuclear charge densities have been accurately measured with electron scattering and have become our picture of the atomic nucleus, see for example [1]. In contrast, our knowledge of neutron densities comes primarily from hadron scattering experiments involving, for example, pions [2], protons [3–5], or antiprotons [6,7], the interpretation of which requires a model-dependent description of the non-perturbative strong interaction. Because of the fact that the weak charge of the neutron is much larger than that of the proton, the measurement of parity violation in electron scattering provides a model-independent probe of neutron densities that is free from most strong-interaction uncertainties [8].

In the Born approximation, the parity-violating cross-section asymmetry for longitudinally polarized electrons elastically scattered from an unpolarized nucleus, A_{PV} , is proportional to the weak form factor $F_W(Q^2)$. This is the Fourier transform of the weak charge density, which is closely related to the neutron density, and therefore, the neutron density can be extracted from an electroweak measurement [8].

$$A_{PV} = \frac{\sigma_R - \sigma_L}{\sigma_R + \sigma_L} \approx \frac{G_F Q^2}{4\pi\alpha\sqrt{2}} \frac{F_W(Q^2)}{F_{ch}(Q^2)}, \quad (1)$$

where $\sigma_{R(L)}$ is the differential cross section for elastic scattering of right (R) and left (L) handed longitudinally polarized electrons, G_F is the Fermi constant, α the fine structure constant, and $F_{ch}(Q^2)$ is the Fourier transform of the known charge density. However, the Born approximation is not valid for a heavy nucleus and Coulomb-distortion effects must be included. These have been accurately calculated [9] because the charge density is well known, and many other details relevant for a practical parity-violation experiment to measure neutron densities have been discussed in a previous publication [10].

One system of particular interest is the doubly-magic nucleus ^{208}Pb , which has 44 more neutrons than protons; some of these extra neutrons are expected to be found in the surface, where they form a neutron-rich skin. The thickness of this skin is sensitive to nuclear dynamics and provides fundamental nuclear structure information.

A number of mean-field-theory models have been developed that agree with the world's body of data on nuclear charge distributions and other nuclear properties [11–15]. For ^{208}Pb , these are consistent with a radius of the point-neutron distribution R_n between 0.0 and 0.4 fm larger than that of the point-proton distribution R_p . In this Letter, we report a first measurement of A_{PV} from ^{208}Pb , which is sensitive to the existence of the neutron skin.

The value of the neutron radius of ^{208}Pb has important implications for models of nuclear structure and their application in atomic physics and astrophysics. There is a strong correlation between R_n of ^{208}Pb and the pressure of neutron matter P at densities near 0.1 fm^{-3} (about 2/3 of nuclear density) [16]. A larger P will push neutrons out against surface tension and increase R_n . Therefore, measuring R_n constrains the equation of state (EOS), the pressure as a function of density, of neutron matter.

The correlation between R_n and the radius of a neutron star r_{NS} is also very interesting [17]. In general, a larger R_n implies a stiffer EOS, with a larger pressure, that will also suggest r_{NS} is larger. Recently, there has been great progress in deducing r_{NS} from x-ray observations. From observations of x-ray bursts, Ozel *et al.* [18] find r_{NS} is very small, near 10 km, implying that the EOS softens at high density which is suggestive of a transition to an exotic phase of QCD. In contrast, Steiner *et al.* [19] conclude that r_{NS} is near 12 km, leading to a prediction that $R_n - R_p = 0.15 \pm 0.02$ fm for ^{208}Pb . This implies a stiffer EOS which leaves little room for softening due to a phase transition at high density.

Recently, Hebeler *et al.* [20] used chiral perturbation theory to calculate the EOS of neutron matter including important contributions from three-neutron forces. From their EOS, they predict $R_n - R_p = 0.17 \pm 0.03$ fm for ^{208}Pb . Monte Carlo calculations by Carlson *et al.* [21] also find sensitivity to three-neutron forces. The measurement of R_n provides an important check of fundamental neutron matter calculations, and constrains three-neutron forces.

The EOS of neutron-rich matter is closely related to the symmetry energy S . There is a strong correlation between

R_n and the density dependence of the symmetry energy $dS/d\rho$, with ρ as the baryon density. The symmetry energy can be probed in heavy-ion collisions [22]. For example, $dS/d\rho$ has been extracted from isospin diffusion data [23] using a transport model.

The symmetry energy S helps determine the composition of a neutron star. A large S at high density would imply a large proton fraction, which would allow the direct Urca process [24] of rapid neutrino cooling. If $R_n - R_p$ in ^{208}Pb were large, it is likely that massive neutron stars would cool quickly by direct Urca. In addition, the transition density from a solid neutron star crust to the liquid interior is strongly correlated with $R_n - R_p$ [25].

Reinhard and Nazarewicz claim that $R_n - R_p$ is tightly correlated with the dipole polarizability α_D [26] and Tamii *et al.* use this correlation to infer $R_n - R_p$ from a new measurement of α_D [27].

Atomic parity violation (APV) is also sensitive to R_n [10,28,29]. A future low-energy test of the standard model may involve the combination of a precise APV experiment along with PV electron scattering to constrain R_n [28]. Alternatively, measuring APV for a range of isotopes could provide information on neutron densities [30].

The measurement was carried out in Hall A at the Thomas Jefferson National Accelerator Facility. The experimental configuration is similar to that used previously for studies of the weak form factor of the proton and ^4He [31–33]. A 50 to 70 μA continuous-wave beam of longitudinally polarized 1.06 GeV electrons was incident on a 0.55 mm thick isotopically pure ^{208}Pb target foil. A 4×4 mm square beam raster prevented the target from melting. Two 150 μm diamond foils sandwiched the lead foil to improve thermal conductance to a copper frame cooled to 20 K with cryogenic helium. Elastically scattered electrons were focused onto thin quartz detectors in the twin High-Resolution Spectrometers (HRS) [34]. The addition of a pair of dipole septum magnets between the target and the HRSs allowed us to achieve a forward scattering angle of $\theta_{\text{lab}} \sim 5^\circ$. The HRS momentum resolution ensured that only elastic events (and a negligible fraction of inelastic events from the 2.6 MeV first excited state) were accepted by the quartz detectors. Cherenkov light from each quartz bar traversed air light guides and were detected by 2-inch quartz-window photomultipliers (PMT).

The polarized electron beam originated from a strained GaAsP photocathode illuminated by circularly polarized light [35]. The accelerated beam was directed into Hall A, where its intensity, energy, polarization, and trajectory on target were inferred from the response of several monitoring devices. The sign of the laser circular polarization determined the electron helicity; this was held constant for periods of 8.33 ms, referred to as “windows”. The integrated responses of detector PMTs and beam monitors were digitized by an 18-bit analog-to-digital converter and

recorded for each window. Two “window quadruplet” patterns of helicity states (+ − − + or − + + −) ensured complementary measurements at the same phase relative to the 60 Hz line power, thus canceling powerline noise from the asymmetry measurement. The right-left helicity asymmetry in the integrated detector response, normalized to the beam intensity, was computed for sets of complementary helicity windows in each quadruplet to form the raw asymmetry A_{raw} . The sequence of these patterns was chosen with a pseudorandom number generator.

Loose requirements were imposed on beam quality, removing periods of position, energy, or beam-intensity instability. No helicity-dependent cuts were applied, leaving a final data sample of 2×10^7 helicity-window quadruplets. The design of the apparatus ensured that, after all corrections, the fluctuations in the fractional difference of the PMT response between a pair of successive windows was dominated by scattered-electron counting statistics for rates up to 1 GHz. This facilitated the ability to achieve an A_{PV} precision significantly better than 100 parts per billion (ppb) in a reasonable length of time. Careful attention to the design and configuration of the photocathode laser optics [36] ensured that spurious beam-induced asymmetries were under control at this level.

Random fluctuations in beam position and energy contributed the largest source of noise beyond counting statistics in A_{raw} . Typical beam jitter in window quadruplets was less than 2 parts per million (ppm) in energy, and 20 μm in position. This noise contribution was reduced by measuring window differences Δx_i using beam position monitors and applying a correction $A_{\text{beam}} = \sum c_i \Delta x_i$. The c_i 's were measured several times each hour from calibration data in which the beam was modulated by using steering coils and an accelerating cavity. The largest of the c_i 's was ~ 50 ppm/ μm . The noise in the resulting $A_{\text{corr}} = A_{\text{raw}} - A_{\text{beam}}$ was 210 (180) ppm per quadruplet, for a beam current of 50 (70) μA , dominated by counting statistics (~ 1 GHz at 70 μA). Nonuniformities in target thickness due to thermal damage caused window-to-window luminosity fluctuations from variations in the target area sampled by the rastered beam, leading to the degradation of A_{corr} by $\sim 40\%$. This source of noise was eliminated by locking the raster pattern frequency to a multiple of the helicity frequency. Low-current calibration data, triggered on individual scattered electrons, were regularly collected to evaluate the thickness of lead relative to diamond.

Sensitivity of A_{corr} to a transverse component of the beam polarization, coupled to the vector analyzing powers (A_T) for ^{208}Pb and ^{12}C , was studied using special runs with fully transverse beam polarization. The symmetry of the detector configuration as well as the measured A_T values (to be published separately) resulted in an upper bound for a possible correction to A_{corr} of 0.2%. The A_{raw} and A_{corr} window-pair distributions for the two complete data samples had negligible non-Gaussian tails over more than

4 orders of magnitude. To test the accuracy of error calculations and general statistical behavior of the data, A_{corr} averages and statistical errors were studied for typical one-hour runs, consisting of ~ 50 k quadruplets each. This set of 316 average A_{corr} values, normalized by the corresponding statistical error, populated a Gaussian distribution of unit variance, as expected.

A half-wave ($\lambda/2$) plate was periodically inserted into the injector laser optical path, reversing the sign of the electron beam polarization relative to both the electronic helicity control signals and the voltage applied to the polarized source laser electro-optics. Roughly equal statistics were collected with this wave plate inserted and retracted, suppressing many possible sources of systematic error. An independent method of helicity reversal was feasible with a pair of Wien spin rotators separated by a solenoid, providing an additional powerful check of systematic control. Reversing the direction of the solenoidal field reversed the electron beam helicity while the beam optics, which depend on the square of the solenoidal magnetic field, were unchanged. The $\lambda/2$ reversal was done about every 12 hours and the magnetic spin reversal was performed every few days. The data set consisting of a period between two successive $\lambda/2$ or magnetic spin reversals is referred to as a ‘‘slug’’.

The spin reversals resulted in cumulative differences in beam position and energy of only 4 nm and 0.6 ppb, respectively, leading to a run averaged $A_{\text{beam}} = -39.0 \pm 5.9$ ppb. The asymmetry in beam charge, corrected by the intensity normalization of A_{raw} , was 84.0 ± 1.3 ppb, with the error determined using the correlation of measured beam intensity to PMT response which demonstrated the beam-intensity monitors were linear to better than 1.5%. Nonlinearity in the PMT response was limited to 1% in bench-tests that mimicked running conditions. As shown in Table I, the values of A_{corr} are consistent within statistical errors for each of the reversal states. The reduced χ^2 for A_{corr} slug averages is close to 1 in every case, indicating that any residual beam-related systematic effects were small and randomized over the time period of $\lambda/2$ reversals. The final result is $A_{\text{corr}} = 594 \pm 50(\text{stat}) \pm 9(\text{syst})$ ppb where the systematic uncertainty includes possible effects from A_{beam} , nonlinearity in the detectors or beam charge monitors, and transverse asymmetry. The physics

TABLE I. Values of A_{corr} and the statistical error, for each helicity reversal state and for the grand average. The χ^2 per degree of freedom for each average is also shown.

$\lambda/2$ plate	Spin rotator	A_{corr} (ppb)	δA_{corr} (ppb)	$\chi^2/\text{d.o.f.}$
OUT	RIGHT	606	113	1.03
IN	RIGHT	492	107	0.74
OUT	LEFT	565	95	1.12
IN	LEFT	687	92	1.03
Average		594	50	0.99

asymmetry A_{PV} is formed from A_{corr} by correcting for the beam polarization P_b and background fractions f_i with asymmetries A_i

$$A_{\text{PV}} = \frac{1}{P_b} \frac{A_{\text{corr}} - P_b \sum_i A_i f_i}{1 - \sum_i f_i}. \quad (2)$$

These corrections are summarized in Table II.

The fraction of the accepted flux from ^{12}C in the detectors varied with time due to changes in the target; averaged over the run, the fraction $f = (6.3 \pm 0.6)\%$. The asymmetry of this background was determined to be $A_{\text{PV}}^C = 817 \pm 41$ ppb using the $e-N$ weak neutral isoscalar coupling with standard electroweak corrections [37] and the measured kinematics, with the uncertainty bounded by the precision measurement of A_{PV} from ^4He [31]. This was the only non-negligible background. An additional possible systematic error in $\langle Q^2 \rangle$ lay in the determination of the absolute value of θ_{lab} . A nuclear recoil technique using a water cell target [32] limited the scale error on $\langle Q^2 \rangle$ to 1%.

The spectrometer acceptance function $\epsilon(\theta)$ characterizes the probability, as a function of scattering angle θ , for an electron to reach the detector after elastically scattering from ^{208}Pb . For example, the asymmetry averaged over the acceptance would be

$$\langle A \rangle = \frac{\int d\theta \sin\theta A(\theta) \frac{d\sigma}{d\Omega} \epsilon(\theta)}{\int d\theta \sin\theta \frac{d\sigma}{d\Omega} \epsilon(\theta)}, \quad (3)$$

where $\frac{d\sigma}{d\Omega}$ is the cross section. See Supplemental Material [38] for the acceptance function $\epsilon(\theta)$. The observed distribution of events corrected for the cross section, the background from the carbon (diamond) backing, and the effects of multiple scattering is used to extract $\epsilon(\theta)$; corrections for energy loss in the target were negligible. To compare to predictions, one must integrate the theoretical asymmetry and the Q^2 over $\epsilon(\theta)$. The systematic error in $\epsilon(\theta)$ was evaluated from reasonable variations in the parameters of the simulation and resulted in an additional equivalent error in $\langle Q^2 \rangle$ of 0.8%. Added in quadrature to the error arising from knowledge of $\langle \theta \rangle$, we obtain an overall error in $\langle Q^2 \rangle$ of 1.3%. We do not include this uncertainty in the total systematic uncertainty of the asymmetry. Using a calculation by Horowitz [9], dA_{PV}/dQ^2 is approximately

TABLE II. Corrections to A_{PV} and systematic errors.

Correction	Absolute (ppb)	Relative(%)
Beam Charge Normalization	-84.0 ± 1.5	-12.8 ± 0.2
Beam Asymmetries A_{beam}	39.0 ± 7.2	5.9 ± 1.1
Target Backing	-8.8 ± 2.6	-1.3 ± 0.4
Detector Nonlinearity	0 ± 7.6	0 ± 1.2
Transverse Asymmetry	0 ± 1.2	0 ± 0.2
Polarization P_b	70.9 ± 8.3	10.8 ± 1.3
Total	17.1 ± 13.7	$2.6 \pm 2.1\%$

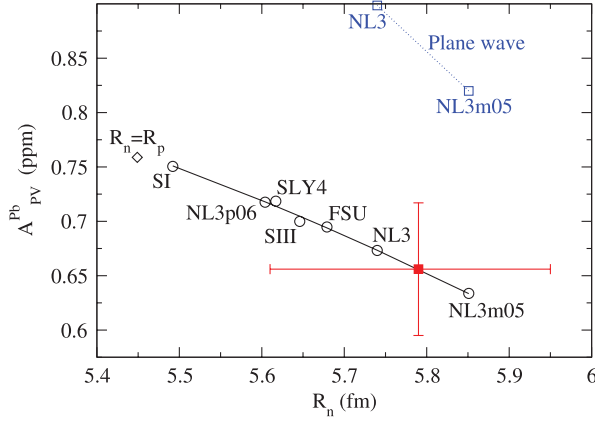


FIG. 1 (color). Result of this experiment (red square) vs neutron point radius R_n in ^{208}Pb . Distorted-wave calculations for seven mean-field neutron densities are circles while the diamond marks the expectation for $R_n = R_p$ [39]. References: NL3m05, NL3, and NL3p06 from [11], FSU from [12], SIII from [13], SLY4 from [14], SI from [15]. The blue squares show plane wave impulse approximation results.

30 ppm/GeV², which would correspond to an additional systematic uncertainty on $A_{\text{PV}}^{\text{Pb}}$ of 3 ppb (0.5% of $A_{\text{PV}}^{\text{Pb}}$).

The beam polarization was continuously monitored by a Compton polarimeter. Helicity-dependent asymmetries in the integrated signal from backscattered Compton photons yielded $P_b = (88.2 \pm 0.1 \pm 1.0)\%$ averaged over the duration of the run. The beam polarization was stable within systematic errors. An independent Møller polarimeter making nine measurements at different times during the run gave $P_b = (90.3 \pm 0.1 \pm 1.1)\%$. We used an average of these two measurements, $P_b = (89.2 \pm 1.0)\%$ which conservatively accounts for the correlated systematic errors between the two measurements.

After all corrections,

$$A_{\text{PV}}^{\text{Pb}} = 656 \pm 60(\text{stat}) \pm 14(\text{syst}) \text{ ppb},$$

at $\langle Q^2 \rangle = 0.00880 \pm 0.00011 \text{ GeV}^2$. This result is displayed in Fig. 1, in which models predicting the point-neutron radius illustrate the correlation of $A_{\text{PV}}^{\text{Pb}}$ and R_n [39].

Seven nonrelativistic and relativistic mean-field models [12–15] were chosen that have charge densities and binding energies in good agreement with experiment, and that span a large range in R_n . The weak charge density ρ_w was calculated from model point-proton ρ_p and neutron ρ_n densities, $\rho_w(r) = q_p \rho_{\text{ch}}(r) + q_n \int d^3 r' [G_E^p \rho_n + G_E^n \rho_p]$, using proton $q_p = 0.0721$ and neutron $q_n = -0.9878$ weak charges that include radiative corrections. Here G_E^p (G_E^n) is the Fourier transform of the proton (neutron) electric form factor. The Dirac equation was solved [9] for an electron scattering from ρ_w and the experimental ρ_{ch} [1], and the resulting $A_{\text{PV}}(\theta)$ integrated over the acceptance, Eq. (3), to yield the open circles in Fig. 1. The importance of Coulomb distortions is emphasized by in-

dicating results from plane-wave calculations, which are not all contained within the vertical axis range of the figure. A least squares fit of the model results yields $R_n \approx 6.156 + 1.675\langle A \rangle - 3.420\langle A \rangle^2 \text{ fm}$ (with $\langle A \rangle$ in ppm), as illustrated. Comparing this to the measured $A_{\text{PV}}^{\text{Pb}}$ implies a value for $R_n = 5.78^{+0.16}_{-0.18} \text{ fm}$. More details of this analysis, along with additional information such as the weak charge form factor and weak radius, will be presented in a future publication [40].

Assuming a point-proton radius of 5.45 fm [41], corresponding to the measured charge radius of 5.50 fm [1], implies that the neutron distribution is 1.8σ larger than that of the protons: $R_n - R_p = 0.33^{+0.16}_{-0.18} \text{ fm}$ [39] (see also [42]). A future run is planned which will reduce the quoted uncertainty by a factor of 3 [43], to discriminate between models and allow predictions relevant for the description of neutron stars and parity violation in atomic systems.

We wish to thank the entire staff of JLab for their efforts to develop and maintain the polarized beam and the experimental apparatus. This work was supported by the U.S. Department of Energy, the National Science Foundation, and from the French CNRS/IN2P3 and ANR. Jefferson Science Associates, LLC, operates Jefferson Lab for the U.S. DOE under U.S. DOE Contract No. DE-AC05-06OR23177.

*Deceased.

†Now at Technische Universitaet Muenchen, Excellence Cluster Universe, Garching b. Muenchen, Germany

*souder@physics.syr.edu

- [1] B. Frois *et al.*, *Phys. Rev. Lett.* **38**, 152 (1977).
- [2] C. Garcia-Recio, J. Nieves, and E. Oset, *Nucl. Phys.* **A547**, 473 (1992).
- [3] L. Ray, W. R. Coker, and G. W. Hoffmann, *Phys. Rev. C* **18**, 2641 (1978).
- [4] V. E. Starodubsky and N. M. Hintz, *Phys. Rev. C* **49**, 2118 (1994).
- [5] B. C. Clark, L. J. Kerr, and S. Hama, *Phys. Rev. C* **67**, 054605 (2003).
- [6] A. Trzcinska *et al.*, *Phys. Rev. Lett.* **87**, 082501 (2001).
- [7] H. Lenske, *Hyperfine Interact.* **194**, 277 (2009).
- [8] T. W. Donnelly, J. Dubach, and I. Sick, *Nucl. Phys.* **A503**, 589 (1989).
- [9] C. J. Horowitz, *Phys. Rev. C* **57**, 3430 (1998).
- [10] C. J. Horowitz, S. J. Pollock, P. A. Souder, and R. Michaels, *Phys. Rev. C* **63**, 025501 (2001).
- [11] G. A. Lalazissis, J. Konig, and P. Ring, *Phys. Rev. C* **55**, 540 (1997).
- [12] B. G. Todd-Rutel and J. Piekarewicz, *Phys. Rev. Lett.* **95**, 122501 (2005).
- [13] M. Beiner, H. Flocard, N. van Giai, and P. Quentin, *Nucl. Phys.* **A238**, 29 (1975).
- [14] E. Chabanat, P. Bonche, P. Haensel, J. Meyer, and R. Schaeffer, *Nucl. Phys.* **A635**, 231 (1998).
- [15] D. Vautherin and D. M. Brink, *Phys. Rev. C* **5**, 626 (1972).
- [16] B. A. Brown, *Phys. Rev. Lett.* **85**, 5296 (2000).

- [17] C.J. Horowitz and J. Piekarewicz, *Phys. Rev. C* **64**, 062802 (2001).
- [18] F. Ozel, G. Baym, and T. Guver, *Phys. Rev. D* **82**, 101301 (2010).
- [19] A. W. Steiner, J. M. Lattimer, and E. F. Brown, *Astrophys. J.* **722**, 33 (2010).
- [20] K. Hebeler, J. M. Lattimer, C. J. Pethick, and A. Schwenk, *Phys. Rev. Lett.* **105**, 161102 (2010).
- [21] S. Gandolfi, J. Carlson, and S. Reddy, [arXiv:1101.1921](https://arxiv.org/abs/1101.1921).
- [22] W. G. Lynch *et al.*, *Prog. Part. Nucl. Phys.* **62**, 427 (2009).
- [23] M. B. Tsang *et al.*, *Phys. Rev. Lett.* **102**, 122701 (2009).
- [24] C.J. Horowitz and J. Piekarewicz, *Phys. Rev. C* **66**, 055803 (2002).
- [25] C.J. Horowitz and J. Piekarewicz, *Phys. Rev. Lett.* **86**, 5647 (2001).
- [26] P.G. Reinhard and W. Nazarewicz, *Phys. Rev. C* **81**, 051303 (2010).
- [27] A. Tamii *et al.*, *Phys. Rev. Lett.* **107**, 062502 (2011).
- [28] S.J. Pollock, E.N. Fortson, and L. Wilets, *Phys. Rev. C* **46**, 2587 (1992); S.J. Pollock and M.C. Welliver, *Phys. Lett. B* **464**, 177 (1999).
- [29] B. A. Brown, A. Derevianko, and V. V. Flambaum, *Phys. Rev. C* **79**, 035501 (2009).
- [30] K. Tsigutkin *et al.*, *Phys. Rev. A* **81**, 032114 (2010).
- [31] A. Acha *et al.*, *Phys. Rev. Lett.* **98**, 032301 (2007).
- [32] K. A. Aniol *et al.*, *Phys. Rev. Lett.* **96**, 022003 (2006).
- [33] K. A. Aniol *et al.*, *Phys. Rev. C* **69**, 065501 (2004).
- [34] J. Alcorn *et al.*, *Nucl. Instrum. Methods Phys. Res., Sect. A* **522**, 294 (2004).
- [35] C.K. Sinclair *et al.*, *Phys. Rev. ST Accel. Beams* **10**, 023501 (2007); P.A. Adderley *et al.*, *Phys. Rev. ST Accel. Beams* **13**, 010101 (2010).
- [36] K.D. Paschke, *Eur. Phys. J. A* **32**, 549 (2007).
- [37] K. Nakamura, *et al.* (Particle Data Group) *J. Phys. G* **37**, 075021 (2010).
- [38] See Supplemental Material at <http://link.aps.org/supplemental/10.1103/PhysRevLett.108.112502> for the acceptance function $\epsilon(\theta)$ to be used in Eq. (3)
- [39] S. Ban, C. J. Horowitz, and R. Michaels, *J. Phys. G* **39**, 015104 (2012).
- [40] C.J. Horowitz *et al.*, [arXiv:1202.1468](https://arxiv.org/abs/1202.1468).
- [41] A. Ong, J. C. Berengut, and V. V. Flambaum, *Phys. Rev. C* **82**, 014320 (2010).
- [42] X. Roca-Maza, M. Centelles, X. Vinas, and M. Warda, *Phys. Rev. Lett.* **106**, 252501 (2011).
- [43] Jefferson Lab Experiment E12-11-101 (PREX-II). Proposal available at <http://hallaweb.jlab.org/parity/prex>.